2009

# Reduction of Calcium Release Site Models via Fast/Slow Analysis and Iterative Aggregation/Disaggregation

Yan Hao

Peter Kemper

Gregory D. Smith
*William & Mary*, gdsmit@wm.edu



## Recommended Citation

Hao, Yan; Kemper, Peter; and Smith, Gregory D., Reduction of Calcium Release Site Models via Fast/Slow Analysis and Iterative Aggregation/Disaggregation (2009). *Chaos: An Interdiscipliary Journal of Nonlinear Science*, 19(3).
https://doi.org/10.1063/1.3223663

# Reduction of calcium release site models via fast/slow analysis and iterative aggregation/disaggregation

Yan Hao,[1] Peter Kemper,[2] and Gregory D. Smith[1]
[1]*Department of Applied Science, College of William and Mary, Williamsburg, Virginia 23187, USA*
[2]*Department of Computer Science, College of William and Mary, Williamsburg, Virginia 23187, USA*

(Received 15 February 2009; accepted 17 August 2009; published online 18 September 2009)

Mathematical models of calcium release sites derived from Markov chain models of intracellular calcium channels exhibit collective gating reminiscent of the experimentally observed phenomenon of calcium puffs and sparks. Such models often take the form of stochastic automata networks in which the transition probabilities of each channel depend on the local calcium concentration and thus the state of the other channels. In order to overcome the state-space explosion that occurs in such compositionally defined calcium release site models, we have implemented several automated procedures for model reduction using fast/slow analysis. After categorizing rate constants in the single channel model as either fast or slow, groups of states in the expanded release site model that are connected by fast transitions are lumped, and transition rates between reduced states are chosen consistent with the conditional probability distribution among states within each group. For small problems these conditional probability distributions can be numerically calculated from the full model without approximation. For large problems the conditional probability distributions can be approximated without the construction of the full model by assuming rapid mixing of states connected by fast transitions. Alternatively, iterative aggregation/disaggregation may be employed to obtain reduced calcium release site models in a memory-efficient fashion. Benchmarking of several different iterative aggregation/disaggregation-based fast/slow reduction schemes establishes the effectiveness of automated calcium release site reduction utilizing the Koury–McAllister–Stewart method. © *2009 American Institute of Physics*. [DOI: 10.1063/1.3223663]

**Mathematical modeling has played an important role in understanding the relationship between single channel gating of intracellular calcium ($Ca^{2+}$) channels and the stochastic dynamics of $Ca^{2+}$ release events known as $Ca^{2+}$ puffs and sparks. $Ca^{2+}$ release site models are defined by the composition of single channel models whose transition probabilities depend on the local calcium concentration and thus the state of the other channels. Because the large state space of such models impedes computational analysis of the dynamics of $Ca^{2+}$ release sites, we implement and validate the application of several automated model reduction techniques that leverage separation of time scales, a common feature of single channel models of inositol 1,4,5-trisphosphate receptors ($IP_3Rs$) and ryanodine receptors (RyRs). The authors show for the first time that memory-efficient iterative aggregation/disaggregation (IAD)-based numerical schemes are effective for fast/slow reduction in compositionally defined $Ca^{2+}$ release site models.**

## I. INTRODUCTION

Localized intracellular $Ca^{2+}$ elevations known as puffs and sparks arise from the concerted gating of $IP_3Rs$ and RyRs, intracellular $Ca^{2+}$ channels that are clustered at release sites on the surface of the endoplasmic reticulum or sarcoplasmic reticulum.[1–7] When Markov chain models of these intracellular $Ca^{2+}$-regulated $Ca^{2+}$ channels are coupled via a mathematical representation of a $Ca^{2+}$ microdomain, simulated $Ca^{2+}$ release sites may exhibit the phenomenon of "stochastic $Ca^{2+}$ excitability" where channels open and close in a concerted fashion reminiscent of $Ca^{2+}$ puffs and sparks.[8,9] Detailed modeling and analysis of the stochastic dynamics of $Ca^{2+}$ release have helped to develop our understanding of the relationship between single channel kinetics and emergent phenomena that lead to localized $Ca^{2+}$ elevations such as $Ca^{2+}$ puffs and sparks.[9–19] However, the state-space explosion that results when $Ca^{2+}$ release site models are compositionally defined in terms of single channel models is a challenge to physiologically realistic modeling of the stochastic dynamics of $Ca^{2+}$ release.[8,20]

Quasistatic approximation based on a separation of time scales is a well-established approach to reducing single channel models of $Ca^{2+}$-regulated $Ca^{2+}$ channels. Ordinary differential equation (ODE) models of the dynamics of whole cell $Ca^{2+}$ responses are often reduced through the observation that $Ca^{2+}$ activation of $IP_3Rs$ or RyRs is a faster process than $Ca^{2+}$-dependent or independent inactivation. For example, the four-state Keizer–Levine[21] RyR model shown in Fig. 1 can be reduced to a two-state model that can be represented by a single Hodgkin–Huxley-style gating variable in whole cell models of $Ca^{2+}$ oscillations, because the $C_1 \leftrightarrow O_2$ and $O_2 \leftrightarrow O_3$ transitions are fast compared to the $O_2 \leftrightarrow C_4$ transitions. Similarly, the well-known eight-state De Young–Keizer[22] $IP_3R$ subunit model can be reduced to two states by assuming both $IP_3$ potentiation and $Ca^{2+}$ activation are fast compared to $Ca^{2+}$ inactivation.[23]

 

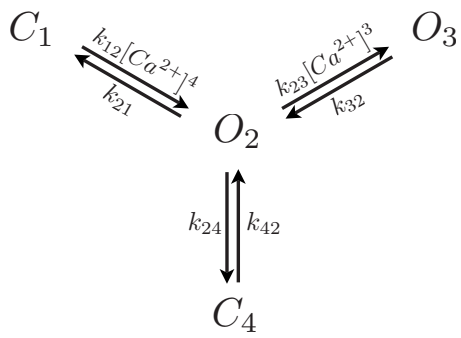


FIG. 1. State-transition diagram for the Keizer–Levine RyR model (Ref. 21). This model includes two closed ($C_1$ and $C_4$) and two open ($O_2$ and $O_3$) states. The $C_1 \to O_2$ and $O_2 \to O_3$ transitions involve binding of four and three $Ca^{2+}$ ions, respectively, while the other transitions do not involve $Ca^{2+}$. Parameters as in Ref. 21: $k_{12}=1500\ \mu M^{-4}\ s^{-1}$; $k_{23}=1500\ \mu M^{-3}\ s^{-1}$; in $s^{-1}$: $k_{21}=28.8$, $k_{32}=385.9$, $k_{24}=1.75$, and $k_{42}=0.1$.

The fast/slow analysis that occurs in many ODE models of intracellular $Ca^{2+}$ responses is straightforward because the intracellular channels are coupled to the bulk cytosolic $[Ca^{2+}]$, the dynamics of which are assumed to be slow compared to the fast transitions within identified groups of states (e.g., $C_1$, $O_2$, and $O_3$ in Fig. 1). While fast/slow reduction can be applied to Markov chain models of $Ca^{2+}$ release sites, the kinetics of domain $Ca^{2+}$ near clusters of intracellular channels are considerably faster than the kinetics of bulk $Ca^{2+}$ (milliseconds as opposed to seconds). Consequently, in the release site models that are the focus of this paper, the domain $[Ca^{2+}]$ is assumed to be an instantaneous function of the number of open channels at a release site. That is, domain $Ca^{2+}$ is not an environmental variable extrinsic to the $Ca^{2+}$ release site model, but rather an intrinsic aspect of the model that is algebraically determined from the current release site state.[10,12,19,24] The focus of this paper is the implementation and validation of automated fast/slow reduction procedures for this particular class of $Ca^{2+}$ release site models, which are large structured time-homogeneous Markov chains.

The remainder of this paper is organized as follows. In Secs. II and III we motivate our model formulation and show a representative simulation of a $Ca^{2+}$ release site composed of multiple Keizer–Levine RyRs interacting via a common domain $[Ca^{2+}]$. In Secs. IV and V we demonstrate and validate fast/slow reduction in compositionally defined $Ca^{2+}$ release site models. Importantly, the conditional probability distributions required for fast/slow reduction can be numerically approximated without the construction of the full model, resulting in a memory-efficient implementation. In Secs. VI and VII we show how IAD methods can be employed to obtain a reduced $Ca^{2+}$ release site model through exact calculation of the required conditional probability distributions. In Sec. VIII we show how a fast/slow reduced $Ca^{2+}$ release site model can be used to efficiently compute puff/spark statistics, such as the probability distribution of the time required to achieve a specified number of refractory channels after a step increase in $[Ca^{2+}]$. Section IX discusses limitations and possible extensions this approach to reduction in $Ca^{2+}$ release site models.

## II. MODEL FORMULATION

Stochastic models of single channel gating often take the form of continuous-time discrete-state Markov chains (for review see Refs. 25 and 26). For example, Fig. 1 shows the state-transition diagram for the four-state Keizer–Levine RyR that includes both fast $Ca^{2+}$ activation and slower $Ca^{2+}$-independent inactivation.[21] Under the assumption that domain $[Ca^{2+}]$ changes are fast compared to channel transitions, this single channel model is continuous-time Markov chain with infinitesimal generator matrix $\boldsymbol{Q}=(q_{ij})$ given by

$$\boldsymbol{Q}=\begin{bmatrix} \diamondsuit & k_{12}c_\infty^4 & 0 & 0 \\ k_{21} & \diamondsuit & k_{23}(c_\infty+c_*)^3 & k_{24} \\ 0 & k_{32} & \diamondsuit & 0 \\ 0 & k_{42} & 0 & \diamondsuit \end{bmatrix}, \tag{1}$$

where the states have been ordered $C_1$, $O_2$, $O_3$, and $C_4$. The off-diagonal entries of the $\boldsymbol{Q}$-matrix for this irreducible and time-homogeneous Markov chain are transition rates defined by

$$q_{ij}=\lim_{\Delta t\to 0}\frac{1}{\Delta t}\Pr[S(t+\Delta t)=j|S(t)=i], \tag{2}$$

where $i\neq j$ and $S(t)\in\{1,2,3,4\}$ indicates the state of the stochastically gating channel at time $t$. The diamonds on the diagonal entries of the $\boldsymbol{Q}$-matrix indicate values leading to row sums of zero, $q_{ii}=-\Sigma_{j\neq i}q_{ij}<0$. Note that the rate constants $k_{24}$ (and $k_{42}$) for $Ca^{2+}$-independent inactivation of the RyR (and recovery from inactivation) have units of $\text{time}^{-1}$. The dissociation rate constants $k_{21}$ and $k_{32}$ also have units of $\text{time}^{-1}$. The association rate constants $k_{23}$ and $k_{12}$ have units of $\text{conc}^{-\eta}\ \text{time}^{-1}$ where $\eta=3$ or 4 is the cooperativity for $Ca^{2+}$ binding to the regulatory site of the channel. Consistent with the assumption of fast $[Ca^{2+}]$ changes, the background $[Ca^{2+}]$ denoted by $c_\infty$ is used for the $C_1\to O_2$ transition, while the concentration $c_\infty+c_*$ is used for the $O_2\to O_3$ transition. The parameter $c_*$ denotes the elevation over background $Ca^{2+}$ experienced by the $Ca^{2+}$ regulatory site of the channel when the channel is open.

Using the parameters of Fig. 1, $c_\infty=0.1\ \mu M$, and $c_*=0.065\ \mu M$, the equilibration rates for the three pairs of states in the Keizer–Levine RyR model are $k_{12}c_\infty^4+k_{21}=28.9\ s^{-1}$ $(C_1\leftrightarrow O_2)$, $k_{23}(c_\infty+c_*)^3+k_{32}=393\ s^{-1}$ $(O_2\leftrightarrow O_3)$, and $k_{24}+k_{42}=1.85\ s^{-1}$ $(O_2\leftrightarrow C_4)$. The solid lines of Fig. 2(a) correspond to the fast $C_1\leftrightarrow O_2\leftrightarrow O_3$ transitions in the Keizer–Levine RyR, while the dotted line corresponds to the slow $O_2\leftrightarrow C_4$ transition.

All of the statistical properties of the Keizer–Levine RyR can be calculated from its $\boldsymbol{Q}$-matrix [Eq. (1)]. For example, the conditional probability of finding the channel in state $j$ at time $t$ provided it was in state $i$ at time zero is

$$p_{ij}(t)=[e^{t\boldsymbol{Q}}]_{ij}=\Pr[S(t)=j|S(0)=i], \tag{3}$$

where $t\geq 0$ and $[e^{t\boldsymbol{Q}}]_{ij}$ indicates the element in the $i$th row and $j$th column of the matrix exponential. In fact, because the Markov chain is time homogeneous, $\Pr[S(t+s)=j\,|\,S(s)=i]=p_{ij}(t)$ for all $t\geq 0$ and $s\geq 0$.

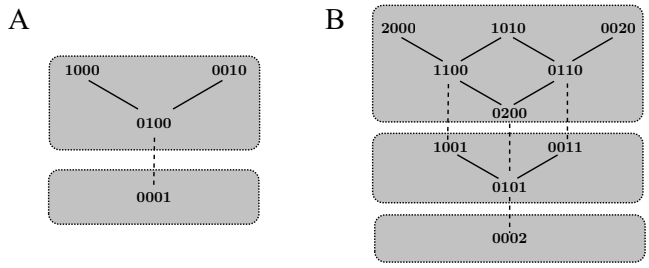


FIG. 2. (a) Topology of the four-state Keizer–Levine RyR model showing fast and slow transitions (solid and dotted lines, respectively). (b) Topology for the ten-state release site composed of two Keizer–Levine RyRs. Gray boxes indicate groups of states connected by fast transitions. The ordered $M$-tuples $(N_1,N_2,\ldots,N_M)$ satisfy $N_i\in\{0,\ldots,N\}$ and $\Sigma_i N_i=N$ where $N_i=n$ indicates $n$ channels in state $i$.

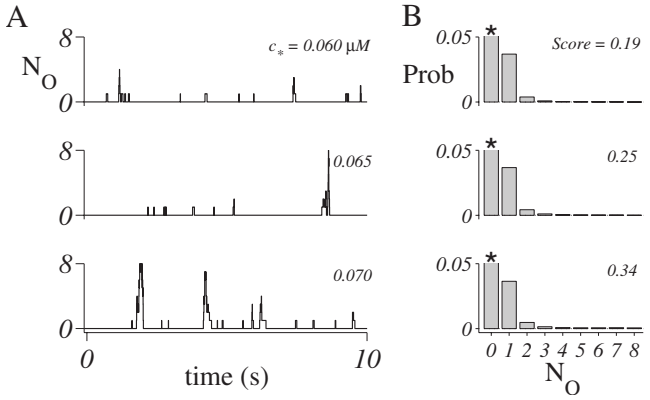


FIG. 3. (a) Representative $Ca^{2+}$ release site simulations involving eight Keizer–Levine RyRs instantaneously coupled via a domain $[Ca^{2+}]$ given by $c=c_\infty+N_O c_*$ where $c_\infty=0.1\ \mu M$ and $c_*=0.06$ (top), 0.065 (middle), and 0.07 $\mu M$ (bottom). When the coupling strength $c_*$ is sufficiently large, the stochastic dynamics of the number of open channels at a release site $(N_O)$ is reminiscent of puffs/sparks. (b) Probability distribution of the number of open channels directly calculated from the generator matrix of the $Ca^{2+}$ release site Markov chain models and the corresponding puff/spark Score of 0.19 (top), 0.25 (middle), and 0.34 (bottom). Asterisks indicate truncated bar for $\Pr[N_O=0]=0.9576$ (top), 0.9561 (middle), and 0.9537 (bottom).

The $Ca^{2+}$ release site models that are the focus of this paper involve $N$ identical Keizer–Levine RyRs interacting via changes in local $[Ca^{2+}]$ under the assumption of "instantaneous mean-field coupling."[8,10,11] That is, we assume that the increase in local $[Ca^{2+}]$ experienced by each channel is an instantaneous function of the number of open channels $(N_O)$,

$$[Ca^{2+}](t)=c_\infty+c_* N_O(t). \tag{4}$$

Because identical channels coupled in this manner are indistinguishable, a release site composed of $N$ $M$-state channels includes

$$\beta(N,M)=\binom{N+M-1}{N}=\frac{(N+M-1)!}{N!\,(M-1)!} \tag{5}$$

distinct states. Each of the $\beta(N,M)$ states can be written as the ordered $M$-tuple $(N_1,N_2,\ldots,N_M)$, where $N_i=n$ indicates $n$ channels in state $i$, $N_i\in\{0,\ldots,N\}$, and $\Sigma_i N_i=N$. Figure 2(b) uses this notation to illustrate the topology of a ten-state $Ca^{2+}$ release site model composed of two coupled Keizer–Levine RyRs. In this case the states take the form $(N_{C_1},N_{O_2},N_{O_3},N_{C_4})$ and, for example, the rate for the $2000\rightarrow 1100$ transition is given by

$$N_{C_1}k_{12}(c_\infty+N_O c_*)^4=2k_{12}c_\infty^4,$$

where $N_O=N_{O_2}+N_{O_3}=0$ and $N_{C_1}=2$ accounts for the fact that either one of the two channels can make a $C_1\rightarrow O_2$ transition. Similarly, the rate for the $0110\rightarrow 0020$ transition is given by

$$N_{O_2}k_{23}(c_\infty+N_O c_*)^3=k_{23}(c_\infty+2c_*)^3$$

because $N_{O_2}=1$ and $N_O=N_{O_2}+N_{O_3}=2$. Consistent with Fig. 2(a), the solid and dotted lines in Fig. 2(b) indicate those transitions associated with fast $Ca^{2+}$-dependent activation and slow $Ca^{2+}$-independent inactivation, respectively.

## III. REPRESENTATIVE CALCIUM RELEASE SITE SIMULATIONS

Figure 3(a) shows the stochastic dynamics of a $Ca^{2+}$ release site composed of eight identical Keizer–Levine RyRs coupled in the fashion described in Sec. II. In each of the three simulations shown, the single channel model parameters follow Fig. 1, the background $[Ca^{2+}]$ is $c_\infty=0.1\ \mu M$, and simulations are performed using the exact numerical method attributed to Gillespie.[27] When the coupling strength $c_*$ is relatively small (0.06 $\mu M$, top panel), increases in the number of open channels usually involve one or a few $Ca^{2+}$ channels, reminiscent of the experimentally observed phenomena of $Ca^{2+}$ blips and quarks.[28,29] However, when the coupling strength is increased to $c_*=0.065$ and 0.07 $\mu M$ (middle and bottom panels), the stochastic dynamics of the number of open channels at a release site $(N_O)$ becomes more robust and concerted. These events often involve a significant fraction of the channels at the release site. Event durations (100–300 ms) and interevent intervals (20–50 s) are similar to the experimentally observed localized $Ca^{2+}$ elevations known as $Ca^{2+}$ puffs and sparks.

Figure 3(b) shows the steady-state probability distribution of the number of open channels at these simulated $Ca^{2+}$ release sites, that is, $\Pr[N_O=n]$ where $n\in\{0,1,\ldots,N\}$. Note that these distributions are not estimated via Monte Carlo simulation, but rather directly calculated from the stationary distribution of the 165-state expanded Markov chain corresponding to eight coupled Keizer–Levine RyRs [$165=\beta(8,4)$ in Eq. (5)]. That is, after constructing the $\boldsymbol{Q}$ matrix for the $Ca^{2+}$ release site model, we numerically solve

$$\boldsymbol{\pi Q}=\mathbf{0}\quad\text{subject to}\quad\boldsymbol{\pi e}=1, \tag{6}$$

where $\boldsymbol{Q}$ is a $165\times 165$ matrix, $\boldsymbol{\pi}$ is $1\times 165$ row vector, and $\boldsymbol{e}$ is a $165\times 1$ column vector of ones (see Appendix A). Each element of the probability distribution of the number of open channels $(\Pr[N_O=n])$ is then constructed as the sum of the appropriate elements of $\boldsymbol{\pi}$. Note that for the different values of the coupling strength used in Fig. 3(b), only subtle differences in the probability distribution of $N_O$ are visible. On the other hand, the presence or absence of puff/sparks in $Ca^{2+}$ release site simulations such as Fig. 3(a) can be assessed

from $\Pr[N_O=n]$ without recourse to Monte Carlo simulation using a response measure dubbed the puff/spark *Score*,[8]

$$\text{Score} = \frac{\text{Var}[f_O]}{\text{E}[f_O]} = \frac{1}{N}\frac{\text{Var}[N_O]}{\text{E}[N_O]}, \tag{7}$$

where $f_O=N_O/N$ is the fraction of open channels. The puff/spark Score takes values between 0 and 1, and a Score of greater than approximately 0.25 indicates the presence of robust stochastic $Ca^{2+}$ excitability [as in the middle and bottom panels of Fig. 3(b)].

In the $Ca^{2+}$ release site model composed of eight Keizer–Levine RyRs (Fig. 3), higher values of the $Ca^{2+}$ coupling strength ($c_*>0.1\ \mu M$) lead to sparks with physiologically unrealistic duration and ultimately a tonically active release site with low puff/spark Score ($c_*>0.4\ \mu M$, not shown). Of course, release site simulations using a different number of channels ($N$) or a different single channel model lead to results distinct from the representative simulations of Fig. 3. Such modeling has played an important role in understanding the relationship between the single channel gating of intracellular $Ca^{2+}$ channels and the stochastic dynamics of $Ca^{2+}$ puffs and sparks (for review see Ref. 30).

## IV. FAST/SLOW REDUCTION FOR CALCIUM RELEASE SITE MODELS

In the context of ODE modeling of whole cell $Ca^{2+}$ responses, the Keizer–Levine RyR model was reduced from four to two states by observing that transition rates between the disinactivated states ($C_1$, $O_2$, and $O_3$) are much faster than the transition rates to and from the inactivated state $C_2$.[21] Similarly, the four-state Markov chain of Eq. (1) can be reduced to a two-state model,

$$(\text{disinact})C_1 \cup O_2 \cup O_3 \underset{\hat{q}_{21}}{\overset{\hat{q}_{12}}{\rightleftharpoons}} C_4(\text{inact}), \tag{8}$$

where $C_1\cup O_2\cup O_3$ indicates the disinactivated macrostate. While the transition rate from the inactivated state to the disinactivated macrostate in the reduced model can be "read off" the full model ($\hat{q}_{21}=q_{42}$, see Fig. 1), determining the transition rate from the disinactivated macrostate to the inactivated state ($\hat{q}_{12}$), requires an estimate of the steady-state conditional probability of being in state $O_2$ given that the channel is in $C_1\cup O_2\cup O_3$, because the product of this conditional probability and $q_{24}$ gives rate of inactivation in the reduced model. Under the assumption of rapid mixing of disinactivated states, this conditional probability can be found using Hill's diagrammatic method[31] applied to the subgraph $C_1\leftrightarrow O_2\leftrightarrow O_3$ resulting in the expression

$$\Pr[O_2|C_1\cup O_2\cup O_3] = \frac{q_{12}q_{32}}{q_{21}q_{32}+q_{12}q_{32}+q_{12}q_{23}}.$$

Thus,

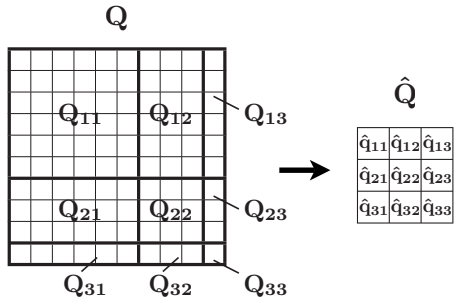


FIG. 4. Partition and contraction of the two-channel Keizer–Levine release site transition matrix. The transition matrix of the original model (left) is partitioned into blocks and corresponds to the groups formed by classifying fast and slow transitions.

$$\hat{q}_{12} = q_{24}\frac{q_{12}q_{32}}{q_{21}q_{32}+q_{12}q_{32}+q_{12}q_{23}} \tag{9}$$

is the required transition rate for disinactivation in the reduced Keizer–Levine RyR [Eq. (8)]. In the reduced single channel model, the open probability conditioned on occupation of the disinactivated macrostate is

$$\Pr[O|C_1\cup O_2\cup O_3] = \frac{q_{12}q_{32}+q_{12}q_{23}}{q_{21}q_{32}+q_{12}q_{32}+q_{12}q_{23}},$$

where $O=O_2\cup O_3$, while the open probability conditioned on occupation of the inactivated state is zero.

Fast/slow reduction for $Ca^{2+}$ release sites composed of several channels can be illustrated by considering $N=2$ Keizer–Levine RyRs coupled via a common domain $[Ca^{2+}]$. As discussed in Sec. III, we assume $[Ca^{2+}](t)=c_\infty+c_*N_O(t)$, where $N_O(t)$ is the number of open channels (0, 1, or 2). Figure 2(b) shows the transition state diagram for two coupled Keizer–Levine RyRs where each release site state is labeled by four digits $n_1n_2n_3n_4$ with $n_i\in\{0,1,2\}$ and $\Sigma_i n_i=2$. As mentioned above, the solid lines correspond to fast $C_1\leftrightarrow O_2\leftrightarrow O_3$ transitions, while the dotted lines correspond to slow $O_2\leftrightarrow C_4$ transitions. The gray boxes of Fig. 2(b) indicate groups of states connected by fast transitions that are good candidates for lumping during a fast/slow reduction procedure that will result in a three-state $Ca^{2+}$ release site model.

As illustrated in Fig. 4, the fast/slow reduction procedure begins by constructing the $\boldsymbol{Q}$-matrix for two coupled channels consistent with the partitioning in Fig. 2(b). The resulting matrix takes the form

$$\boldsymbol{Q} = \begin{bmatrix} \boldsymbol{Q}_{11} & \boldsymbol{Q}_{12} & \boldsymbol{Q}_{13} \\ \boldsymbol{Q}_{21} & \boldsymbol{Q}_{22} & \boldsymbol{Q}_{23} \\ \boldsymbol{Q}_{31} & \boldsymbol{Q}_{32} & \boldsymbol{Q}_{33} \end{bmatrix}, \tag{10}$$

where block $\boldsymbol{Q}_{11}$ is $6\times 6$, block $\boldsymbol{Q}_{22}$ is $3\times 3$, and block $\boldsymbol{Q}_{33}$ is $1\times 1$ (see Fig. 4). To perform the model reduction, we require an estimate of the conditional probability of being in the various substates of each block. Under the assumption of rapid mixing within lumped states, these conditional probability distributions are well approximated by the solutions of the linear systems,

$$\hat{\boldsymbol{\pi}}_i \boldsymbol{Q}_{ii}^{+} = \mathbf{0} \quad \text{subject to} \quad \hat{\boldsymbol{\pi}}_i \boldsymbol{e}_i = 1, \tag{11}$$

where $i \in \{1,2,3\}$. In this expression, $\boldsymbol{Q}_{ii}^{+}$ is given by

$$\boldsymbol{Q}_{ii}^{+} = \boldsymbol{Q}_{ii} + \mathrm{diag}\left( \sum_{j \neq i} \boldsymbol{Q}_{ij} \boldsymbol{e}_j \right), \tag{12}$$

where the sum is over two column vectors, the "diag" operation converts the resulting column vector into a diagonal matrix commensurate with $\boldsymbol{Q}_{ii}$, the unknowns $\hat{\boldsymbol{\pi}}_1$, $\hat{\boldsymbol{\pi}}_2$, and $\hat{\boldsymbol{\pi}}_3$ are $1\times 6$, $1\times 3$, and $1\times 1$, respectively, and the $\boldsymbol{e}_j$ are commensurate column vectors of ones. The approximate conditional probability distributions $\hat{\boldsymbol{\pi}}_i$ are then used to calculate the transition rates between lumped states yielding the reduced model

$$\hat{\boldsymbol{Q}} = \begin{bmatrix} \hat{q}_{11} & \hat{q}_{12} & \hat{q}_{13} \\ \hat{q}_{21} & \hat{q}_{22} & \hat{q}_{23} \\ \hat{q}_{31} & \hat{q}_{32} & \hat{q}_{33} \end{bmatrix}, \tag{13}$$

where

$$\hat{q}_{ij} = \hat{\boldsymbol{\pi}}_i \boldsymbol{Q}_{ij} \boldsymbol{e}_j \tag{14}$$

for $i \neq j$ and $\hat{q}_{ii} = \Sigma_{j\neq i} - \hat{q}_{ij}$. Pseudocode for this fast/slow reduction procedure is presented in Algorithm 1.

**Algorithm 1**: Fast/slow reduction

**require:** $\hat{b}^2$ matrices $\{\boldsymbol{Q}_{ij}\}$ where $\hat{b}$ is size of reduced model

**for** $i = 1, \cdots, \hat{b}$

$\boldsymbol{Q}_{ii}^{+} \leftarrow \boldsymbol{Q}_{ii} + \mathrm{diag}\{\Sigma_{j\neq i} \boldsymbol{Q}_{ij} \boldsymbol{e}_j\}$

solve $\hat{\boldsymbol{\pi}}_i \boldsymbol{Q}_{ii}^{+} = \mathbf{0}$ subject to $\hat{\boldsymbol{\pi}}_i \boldsymbol{e}_i = 1$

**endfor**

**for** $i = 1, \cdots, \hat{b}$

**for** $j = 1, \cdots, i-1, i+1, \cdots, \hat{b}$ **do**

$\hat{q}_{ij} \leftarrow \hat{\boldsymbol{\pi}}_i \boldsymbol{Q}_{ij} \boldsymbol{e}_j$

**endfor**

$\hat{q}_{ii} \leftarrow \Sigma_{j\neq i} - \hat{q}_{ij}$

**endfor**

**return** $\hat{\boldsymbol{Q}} = (\hat{q}_{ij})$

## V. VALIDATION OF FAST/SLOW REDUCTION FOR RELEASE SITES COMPOSED OF SEVERAL CHANNELS

This section validates the numerical approach to fast/slow reduction outlined in Sec. IV using a release site model composed of eight four-state Keizer–Levine RyRs. Mean-field coupling of these channels leads to a $165\times 165$ $\boldsymbol{Q}$-matrix [cf. Eq. (10)] that is partitioned into 81 blocks when states $C_1$, $O_2$, and $O_3$ are lumped. The nine square blocks on the diagonal of the partitioned generator matrix are of size 45, 36, 28, 21, 15, 10, 6, 3, and 1 (see Appendix B). The fast/slow reduction procedure outlined in Algorithm 1 leads to a reduced model specified by the $9\times 9$ matrix $\hat{\boldsymbol{Q}}$ [cf. Eq. (13)].

Perhaps the most straightforward way to validate this approach is to compare the transition probability matrices of the reduced model ($\hat{\boldsymbol{P}} = e^{t\hat{\boldsymbol{Q}}}$) to the transition probability matrix of the full model ($\boldsymbol{P} = e^{t\boldsymbol{Q}}$), see Eq. (3). Assuming the full and reduced models have $b$ and $\hat{b}$ states, respectively, we write

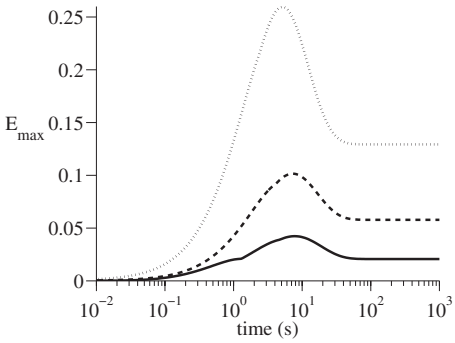


FIG. 5. Error of fast/slow reduction (Algorithm 1) for a release site composed of eight four-state Keizer–Levine RyRs quantified as in Eqs. (15)–(19). Solid, dashed, and dotted lines use $Ca^{2+}$ coupling strengths of $c_* = 0.06$, 0.065, and 0.07 $\mu M$, respectively (cf. Fig. 3). Background $[Ca^{2+}]$ is $c_\infty = 0.1$ $\mu M$ and other parameters are as in Fig. 1.

$$\hat{\boldsymbol{E}}(t) = \hat{\boldsymbol{P}}(t) - \boldsymbol{U}\boldsymbol{P}(t)\boldsymbol{V}, \tag{15}$$

where $\boldsymbol{V}$ is a $b\times\hat{b}$ collector matrix,[32]

$$\boldsymbol{V} = \begin{bmatrix} \boldsymbol{e}_1 & 0 & \cdots & 0 \\ 0 & \boldsymbol{e}_2 & \cdots & 0 \\ \vdots & \vdots & \ddots & \vdots \\ 0 & 0 & \cdots & \boldsymbol{e}_{\hat{b}} \end{bmatrix},$$

the $\boldsymbol{e}_i$ are column vectors of ones with lengths commensurate with $\boldsymbol{Q}_{ii}$, and $\boldsymbol{U}$ is a $\hat{b}\times b$ distributor matrix given by

$$\boldsymbol{U} = \begin{bmatrix} \overline{\boldsymbol{\pi}}_1 & 0 & \cdots & 0 \\ 0 & \overline{\boldsymbol{\pi}}_2 & \cdots & 0 \\ \vdots & \vdots & \ddots & \vdots \\ 0 & 0 & \cdots & \overline{\boldsymbol{\pi}}_{\hat{b}} \end{bmatrix}. \tag{16}$$

The exact conditional probability distributions $\overline{\boldsymbol{\pi}}_i$ that compose $\boldsymbol{U}$ are row vectors given by

$$\overline{\boldsymbol{\pi}}_i = \frac{\boldsymbol{\pi}_i}{\boldsymbol{\pi}_i \boldsymbol{e}_i}, \tag{17}$$

where

$$\boldsymbol{\pi} = [\boldsymbol{\pi}_1, \boldsymbol{\pi}_2, \ldots, \boldsymbol{\pi}_{\hat{b}}] \tag{18}$$

is the conformally partitioned exact stationary distribution of the full model satisfying Eq. (6).

The solid line of Fig. 5 shows the maximum absolute error

$$E_{\max}(t) = \max_{ij} |\hat{\boldsymbol{E}}_{ij}(t)| \tag{19}$$

for a nine-state fast/slow reduced $Ca^{2+}$ release site model obtained by contracting a full model with eight four-state Keizer–Levine RyRs and a coupling strength of $c_* = 0.06$ $\mu M$ [as in the top panel of Fig. 3(a)]. For small

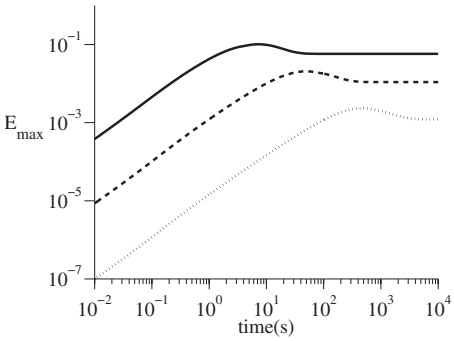


FIG. 6. Logarithmic plot of the error of fast/slow reduction [Eq. (19)] when Algorithm 1 is applied to a release site composed of eight four-state Keizer–Levine RyRs with parameters as in Fig. 5 (solid line). Dashed and dotted lines show that the error of fast/slow reduction is decreased when slow transition rates are decreased by 10 and 100×, respectively. Other parameters as in Fig. 5.

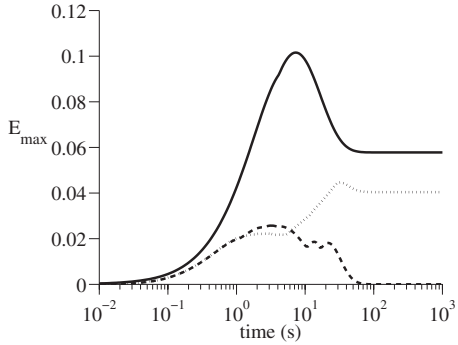


FIG. 7. Error of fast/slow reduction [Eq. (19)] when Algorithms 1 (solid line), 2 (dotted line), and 3 (dashed line) are applied to a release site composed of eight four-state Keizer–Levine RyRs. Parameters: $c_\infty=0.1\ \mu M$, $c_*=0.065\ \mu M$, and as in Fig. 1.

values of $t$ both $\hat{\boldsymbol{P}}$ and $\boldsymbol{P}$ are approximated by identity matrices and consequently $E_{\max}(t)\approx 0$. Note that $E_{\max}(t)$ reaches a peak of 0.05 at $t\approx 10$ s and approaches a limiting value of 0.02 as $t\to\infty$, a value that corresponds to the maximum absolute error of the stationary distribution of the reduced model when compared to the contracted stationary distribution of the full model. [To see this, recall that the columns of $\lim_{t\to\infty}\boldsymbol{P}(t)$ are identical and each row is given by the elements of the stationary probability distribution for the full model that satisfies Eq. (6).] The total absolute error of the stationary distribution of the fast/slow reduced model is $\Sigma_j|\hat{\boldsymbol{E}}_{ij}(\infty)|\approx 0.047$.

The dotted and dashed lines of Fig. 5 show $E_{\max}(t)$ for the fast/slow reduced model when the coupling strength is increased to $c_*=0.065$ and 0.07 $\mu M$ [as in the middle and bottom panels of Fig. 3(a)]. Stochastic $Ca^{2+}$ excitability is more pronounced and the puff/spark Score increases for these values of $c_*$ [see Fig. 3(b)] and both the peak (0.10 and 0.26) and steady state (0.06 and 0.13) errors show a corresponding increase. Perhaps more importantly, Fig. 6 repeats this analysis using the standard value of the $Ca^{2+}$ coupling strength ($c_*=0.065\ \mu M$) and modified parameter sets for the Keizer–Levine RyR model in which the rate of the slow transitions ($k_{24}$ and $k_{42}$) is decreased by 10 and 100× (dashed and dotted lines, respectively). Note that $E_{\max}(t)$ decreases as the separation of time scales between $Ca^{2+}$-dependent activation and $Ca^{2+}$-independent inactivation increases, thereby validating the fast/slow reduction procedure of Algorithm 1.

Because Fig. 5 indicates a significant model reduction error, we considered alternative fast/slow reduction procedures that follow a solution method for nearly completely decomposable Markov chains presented in Stewart's monograph (Ref. 33, pages 285–294). This approach is distinct from Algorithm 1 in that the diagonal elements of the diagonal blocks $\boldsymbol{Q}_{ii}$ of the partitioned generator matrix are not adjusted to remove negative entries corresponding to slow transitions between lumped states [Eq. (11)]. Because the transition rates between macrostates are slow, this is a subtle difference. Nevertheless, Fig. 7 shows a decreased model reduction error using this modified fast/slow reduction procedure (Algorithm 2, dotted line) compared to the previously discussed method (Algorithm 1, solid line). Note that an important step in Algorithm 2 involves solving for the Perron vector of $\boldsymbol{P}_{ii}$, a substochastic matrix given by $\boldsymbol{P}_{ii}=\boldsymbol{I}+\boldsymbol{Q}_{ii}/\delta$ for suitable $\delta$. The Perron vector $\boldsymbol{u}_i$ solves $\boldsymbol{u}_i\boldsymbol{P}_{ii}=\lambda\boldsymbol{u}_i$ subject to $\boldsymbol{u}_i\boldsymbol{e}_i=1$, where $\lambda$ is the spectral radius of $\boldsymbol{P}_{ii}$ (see Appendix A).

**Algorithm 2**: Modified fast/slow reduction

**require:** $\hat{b}^2$ matrices $\{\boldsymbol{Q}_{ij}\}$

**for** $i=1,\cdots,\hat{b}$
  $\delta\leftarrow\max_k|\boldsymbol{Q}_{ii}(k,k)|$
  $\boldsymbol{P}_{ii}\leftarrow\boldsymbol{I}+\boldsymbol{Q}_{ii}/\delta$
  $\boldsymbol{u}_i\leftarrow$ the Perron vector of $\boldsymbol{P}_{ii}$
**endfor**
**for** $i=1,\cdots,\hat{b}$
  **for** $j=1,\cdots,i-1,i+1,\cdots,\hat{b}$
    $\hat{q}_{ij}\leftarrow\hat{\boldsymbol{\pi}}_i\boldsymbol{Q}_{ij}\boldsymbol{e}_j$
  **endfor**
  $\hat{q}_{ii}\leftarrow\Sigma_{j\neq i}-\hat{q}_{ij}$
**endfor**
**return** $\hat{\boldsymbol{Q}}=(\hat{q}_{ij})$

## VI. REDUCTION USING CORRECT CONDITIONAL PROBABILITY IS SUPERIOR TO FAST/SLOW REDUCTION

As discussed in Sec. V, the reduction error obtained using both the original and modified fast/slow reduction methods (Algorithms 1 and 2) is initially zero and asymptotically approaches a finite value as $t\to\infty$ (solid and dotted lines of Fig. 7). As expected, inspection of numerical results associated with Figs. 5–7 confirms that the reduction error is larger when the conditional probability distributions estimated in a block-by-block fashion by Algorithms 1 and 2 become less accurate (not shown). That is, the vector norms

$\|\hat{\boldsymbol{\pi}}_i - \overline{\boldsymbol{\pi}}_i\|$—with $\hat{\boldsymbol{\pi}}_i$ and $\overline{\boldsymbol{\pi}}_i$ given by Eqs. (11) and (17), respectively—are larger when Algorithms 1 and 2 are not performing well. Thus, the error present in the fast/slow reduction approach is potentially avoidable, provided a better approximation of the conditional probability distributions can be obtained.

Equation (5) indicates that a $Ca^{2+}$ release site model composed of eight four-state Keizer–Levine RyRs includes $\beta(8,4)=165$ distinguishable states. For this relatively small release site model, the exact conditional probability distributions $\overline{\boldsymbol{\pi}}_i$ can be calculated using Eqs. (17) and (18) because the numerical solution of the stationary distribution of the full problem is tractable [$\boldsymbol{\pi}$, Eq. (6)]. In this case the rate constants for the reduced model are given by $\hat{q}_{ij}=\overline{\boldsymbol{\pi}}_i\boldsymbol{Q}_{ij}\boldsymbol{e}_j$ for $i\neq j$ [cf. Eq. (14)]. For any given partitioning of states—i.e., the $\hat{b}^2$ matrices $\{\boldsymbol{Q}_{ij}\}$—the reduced model thus obtained will be referred to as the "gold standard" because the conditional probability distributions used to perform the reduction are exactly calculated. While this reduction may not be optimal, the fact that $\hat{\boldsymbol{P}}(\infty)=\boldsymbol{U}\boldsymbol{P}(\infty)\boldsymbol{V}$ [cf. Eq. (15)] means that the error of the gold standard reduced model does at least approach zero as $t\to\infty$. The dashed lines of Fig. 7 show how this important feature of the gold standard reduced model (Algorithm 3) leads to finite integrated error, which is not a property of the other reductions. In addition, the peak value of $\hat{E}_{\max}$ obtained (0.03) is significantly smaller than the results of Algorithms 1 and 2 (0.10 and 0.05, respectively).

**Algorithm 3**: Gold standard reduction with substantial storage requirement

**require:** $\hat{b}^2$ matrices $\{\boldsymbol{Q}_{ij}\}$
solve $\boldsymbol{\pi}\boldsymbol{Q}=\boldsymbol{0}$ subject to $\boldsymbol{\pi}\boldsymbol{e}=1$ where $\boldsymbol{Q}=(\boldsymbol{Q}_{ij})$
**for** $i=1,\cdots,\hat{b}$
  $\overline{\boldsymbol{\pi}}_i \leftarrow \boldsymbol{\pi}_i/\boldsymbol{\pi}_i\boldsymbol{e}_i$ where $\boldsymbol{\pi}=[\boldsymbol{\pi}_1,\boldsymbol{\pi}_2,\cdots,\boldsymbol{\pi}_{\hat{b}}]$
**endfor**
**for** $i=1,\cdots,\hat{b}$
  **for** $j=1,\cdots,i-1,i+1,\cdots,\hat{b}$
    $\hat{q}_{ij}\leftarrow\overline{\boldsymbol{\pi}}_i\boldsymbol{Q}_{ij}\boldsymbol{e}_j$
  **endfor**
  $\hat{q}_{ii}\leftarrow\Sigma_{j\neq i}-\hat{q}_{ij}$
**endfor**
**return** $\hat{\boldsymbol{Q}}=(\hat{q}_{ij})$

Because Algorithm 3 uses the exact conditional probability distributions $\overline{\boldsymbol{\pi}}_i$ [Eq. (17)], its reduction error—the dashed line of Fig. 7—indicates that the time scales of $Ca^{2+}$-dependent activation and $Ca^{2+}$-independent inactivation in the release site model are not completely separated. Figure 8 shows that when this gold standard reduction procedure is repeated using modified parameter sets for the Keizer–Levine RyR model in which the rate of the slow transitions ($k_{24}$ and $k_{42}$) is decreased by 10 and 100×, the peak error decreases from 0.03 to $5.7\times10^{-3}$ and $6.6\times10^{-4}$, respectively (cf. Fig. 6).

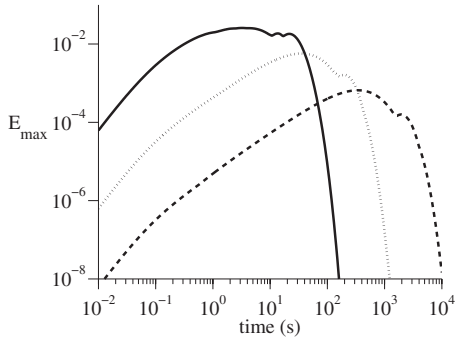


FIG. 8. Logarithmic plot of the error of fast/slow reduction [Eq. (19)] when Algorithm 3 is applied to a release site composed of eight four-state Keizer–Levine RyRs with parameters as in Fig. 5 (solid line). Dotted and dashed lines show a decreased error when the rate of slow transitions is decreased by 10 and 100×, respectively.

## VII. ITERATIVE AGGREGATION/DISAGGREGATION METHODS

Using $Ca^{2+}$ release sites composed of a small number of channels, Sec. VI showed that model reduction using exact conditional probability distributions ($\overline{\boldsymbol{\pi}}$, Algorithm 3) is superior to fast/slow reduction procedures that use approximate conditional probability distributions ($\hat{\boldsymbol{\pi}}$, Algorithms 1 and 2). On the other hand, the storage requirements of Algorithm 3are far in excess of Algorithms 1 and 2. (Recall that Algorithm 3 solves for the full model stationary distribution [Eq. (6)], Algorithm 1 sequentially solves for the stationary distributions of the various blocks of the partitioned generator matrix of the full model [Eq. (11)], and Algorithm 2 sequentially solves for the Perron vectors of $\boldsymbol{P}_{ii}=\boldsymbol{I}+\boldsymbol{Q}_{ii}/\delta$.) Indeed, the substantial storage requirements of Algorithm 3 make it inappropriate as a fast/slow reduction procedure for $Ca^{2+}$ release sites with a large number of states.

IAD methods are a well-known alternative to direct methods for calculating the stationary distribution of large Markov chains.[33] Because these methods often perform well when a Markov chain is irreducible and nearly completely decomposable, we implemented a memory-efficient version

TABLE I. Benchmark calculations using two IAD algorithms: KMS and Vantilborgh. The number of iterations (Iter) before convergence of the iteration vector (tolerance=$10^{-8}$ in Algorithm 4) and the residual (Resid) of the calculated stationary distribution vector $\boldsymbol{\pi}$ given by $\|\boldsymbol{\pi}\boldsymbol{Q}\|_1$ are shown. Parameters: $c_\infty=0.1$ $\mu M$, $c_*=0.06$ $\mu M$, and as in Fig. 1. Because the $Ca^{2+}$ coupling strength is fixed, release sites with large $N$ are tonically active resulting in low puff/spark Score (cf. Table II).

| | KMS | | Vantilborgh | | |
|---|---|---|---|---|---|
| $N$ | Iter | Resid | Iter | Resid | Score |
| 10 | 15 | $1.9\times10^{-10}$ | 15 | $7.4\times10^{-10}$ | 0.35 |
| 20 | 36 | $2.6\times10^{-9}$ | 85 | $2.9\times10^{-8}$ | 0.49 |
| 30 | 33 | $2.3\times10^{-9}$ | 99 | $5.6\times10^{-8}$ | 0.33 |
| 40 | 28 | $2.2\times10^{-9}$ | 73 | $3.8\times10^{-8}$ | 0.23 |
| 50 | 22 | $2.9\times10^{-9}$ | 59 | $4.5\times10^{-8}$ | 0.15 |
| 60 | 13 | $4.5\times10^{-10}$ | 14 | $3.4\times10^{-9}$ | <0.01 |
| 70 | 5 | $1.2\times10^{-9}$ | 8 | $9.4\times10^{-10}$ | <0.01 |
| 80 | 9 | $1.31\times10^{-9}$ | 15 | $1.88\times10^{-9}$ | <0.01 |

of Algorithm 3 that solves for the stationary distribution of the full model using the Koury–McAllister–Stewart (KMS) (Ref. 34) IAD method (see Algorithm 4). For comparison, we also implemented release site reduction procedures that utilize the IAD methods of Vantilborgh and Takahashi (algorithms not shown).[35]

**Algorithm 4**: Reduction using Koury–McAllister–Stewart iterative aggregation/disaggregation

**require:** $\hat{b}^2$ matrices $\{\boldsymbol{Q}_{ij}\}$ and *tolerance*
$\delta \leftarrow \max_i \max_k |\boldsymbol{Q}_{ii}(k,k)|$
**for** $i=1,\cdots,\hat{b}$
  $\boldsymbol{P}_{ii} \leftarrow \boldsymbol{I}+\boldsymbol{Q}_{ii}/\delta$
  $\boldsymbol{y}_i^{(0)} \leftarrow$ row vector of $1/b$ commensurate with $\boldsymbol{P}_{ii}$
  **for** $j=1,\cdots,i-1,i+1,\cdots,\hat{b}$
    $\boldsymbol{P}_{ij} \leftarrow \boldsymbol{Q}_{ij}/\delta$
  **endfor**
**endfor**
$\boldsymbol{y}^{(0)} \leftarrow [\boldsymbol{y}_1^{(0)}, \boldsymbol{y}_2^{(0)}, \cdots, \boldsymbol{y}_{\hat{b}}^{(0)}]$
$m \leftarrow 0$, $change \leftarrow \infty$
**while** $change > tolerance$
  $m \leftarrow m+1$
  **for** $i=1,\cdots,\hat{b}$ **do**
    $\tilde{\boldsymbol{y}}_i^{(m-1)} = \boldsymbol{y}_i^{(m-1)} / \|\boldsymbol{y}_i^{(m-1)}\|_1$
  **endfor**
  **for** $i=1,\cdots,\hat{b}$ **do**
    **for** $j=1,\cdots,\hat{b}$ **do**
      $\boldsymbol{A}^{(m-1)}(i,j) = \tilde{\boldsymbol{y}}_i^{(m-1)} \boldsymbol{P}_{ij} \boldsymbol{e}_j$
    **endfor**
  **endfor**
  solve $\boldsymbol{w}^{(m-1)}(\boldsymbol{A}^{(m-1)}-\boldsymbol{I})=\boldsymbol{0}$
    where $\|\boldsymbol{w}^{(m-1)}\|_1 = 1$
  $\boldsymbol{z}^{(m)} \leftarrow [w_1^{(m-1)}\tilde{\boldsymbol{y}}_1^{(m-1)}, \cdots, w_{\hat{b}}^{(m-1)}\tilde{\boldsymbol{y}}_{\hat{b}}^{(m-1)}]$
  **for** $j=\hat{b},\hat{b}-1,\cdots,1$ **do**
    solve $\boldsymbol{y}_j^{(m)} = \boldsymbol{y}_j^{(m)}\boldsymbol{P}_{jj} + \Sigma_{i<j}\boldsymbol{z}_i^{(m)}\boldsymbol{P}_{ij} + \Sigma_{i>j}\boldsymbol{y}_i^{(m)}\boldsymbol{P}_{ij}$
  **endfor**
  $change \leftarrow \|\boldsymbol{y}^{(m)}-\boldsymbol{y}^{(m-1)}\|_1$
**endwhile**
**return** $\hat{\boldsymbol{Q}} \leftarrow \delta(\boldsymbol{A}^{(m-1)}-1)$ and $\boldsymbol{\pi} \leftarrow \boldsymbol{y}^{(m-1)}$

Table I shows the number of iterations required for convergence of the KMS and Vantilborgh algorithms for $Ca^{2+}$ release sites composed of up to 80 four-state Keizer–Levine RyRs when $c_\infty = 0.1\ \mu M$ and $c_* = 0.06\ \mu M$. The residuals given by $\|\boldsymbol{\pi Q}\|_1$ calculated in a block-by-block fashion from $\{\boldsymbol{\pi}_i\}$ and $\{\boldsymbol{Q}_{ij}\}$ are also shown. Small residuals indicate convergence of the IAD methods to the correct stationary probability distribution $\boldsymbol{\pi}$, yielding the exact conditional probability distributions $\overline{\boldsymbol{\pi}}_i$ [Eq. (18)] and a gold standard reduced model $\hat{\boldsymbol{Q}}=(\hat{q}_{ij})$ where $\hat{q}_{ij}=\overline{\boldsymbol{\pi}}_i \boldsymbol{Q}_{ij} \boldsymbol{e}_j$ for $i \neq j$. Our implementation of the Takahashi IAD method was less successful than the KMS and Vantilborgh methods and did not converge for $N \geq 30$ (not shown).

TABLE II. Benchmark calculations using $c_*$ values chosen so that the puff/spark Score of the full model indicated robust $Ca^{2+}$ excitability. See legend of Table I.

| | KMS | | | |
|---|---|---|---|---|
| $N$ | Iter | Resid | $c_*$ | Score |
| 30 | 44 | $1.7\times10^{-9}$ | 0.04 | 0.50 |
| 30 | 39 | $2.9\times10^{-9}$ | 0.05 | 0.41 |
| 30 | 33 | $2.3\times10^{-9}$ | 0.06 | 0.33 |
| 40 | 53 | $1.7\times10^{-9}$ | 0.03 | 0.51 |
| 40 | 46 | $1.6\times10^{-9}$ | 0.04 | 0.39 |
| 40 | 33 | $3.3\times10^{-9}$ | 0.05 | 0.30 |
| 50 | 57 | $3.3\times10^{-9}$ | 0.03 | 0.44 |
| 50 | 46 | $2.1\times10^{-9}$ | 0.04 | 0.30 |
| 50 | 28 | $4.4\times10^{-9}$ | 0.05 | 0.22 |
| 60 | 97 | $3.01\times10^{-9}$ | 0.02 | 0.52 |
| 60 | 64 | $3.54\times10^{-9}$ | 0.03 | 0.36 |
| 60 | 38 | $1.47\times10^{-9}$ | 0.04 | 0.23 |

Table I shows that the number of iterations required for the KMS and Vantilborgh IAD methods first increases and then decreases as a function of $N$, presumably reflecting the fact that the $Ca^{2+}$ release site dynamics change significantly when $N$ is increased with fixed $c_*$ (note that the puff/spark Score increases and decreases in a similar fashion). In fact, for $N \geq 50$ the low puff/spark Scores in Table I reflect tonically active $Ca^{2+}$ release sites.

To ensure that the success of model reduction using the KMS method for large $N$ is not dependent on the release sites being tonically active, benchmark calculations were repeated using $c_*$ values selected to ensure that the full model exhibited robust $Ca^{2+}$ excitability (Score $>0.25$). Using these parameters, Table II demonstrates successful release site reduction using the KMS method (Algorithm 4) with up to 60 Keizer–Levine RyRs. While the number of iterations required for convergence depends on the $Ca^{2+}$ coupling strength, the residuals are consistently small.

In both Tables I and II, the $N+1$-state reduced $Ca^{2+}$ release site models are contractions of full models with $\beta(N,4)$ states [Eq. (5)]. The largest $Ca^{2+}$ release site model successfully reduced using the KMS IAD method (see Algorithm 4) included $\beta(80,4)=91\,881$ states and $2\times3\beta(80,3)=531\,360$ transitions, where 3 corresponds to the number of edges in the state-transition diagram for the Keizer–Levine RyR [Fig. 2(a)] and $3\beta(80,3)$ is the number of edges in state-transition diagram of the 80-RyR $Ca^{2+}$ release site [cf. Fig. 2(b)].

## VIII. EXAMPLE OF DIRECT CALCULATIONS USING FAST/SLOW REDUCTION

As mentioned in Sec. I, automated fast/slow reduction techniques are of interest because they may facilitate studies of $Ca^{2+}$ release site dynamics that would otherwise be intractable due to the state-space explosion that occurs when multiple single channel models are coupled; below we illustrate this point. The thin solid lines of Fig. 9 show the number of

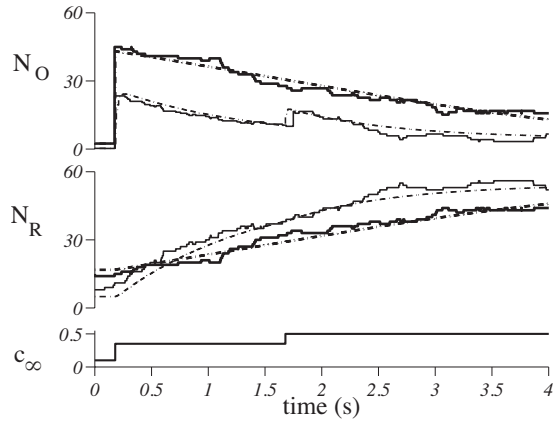


FIG. 9. Monte Carlo simulation (solid lines) and direct calculation (broken lines) of the number of open ($N_O$) and refractory ($N_R$) channels in a stochastic simulation of a $Ca^{2+}$ release site composed of 60 Keizer–Levine RyRs that are either independently gating (thin lines, $c_*=0$) or coupled (thick lines, $c_*=0.02\ \mu M$) following an increase in the background $[Ca^{2+}]$ from $c_\infty=0.1$ to 0.35 and subsequently to 0.5 $\mu M$ (bottom panel).

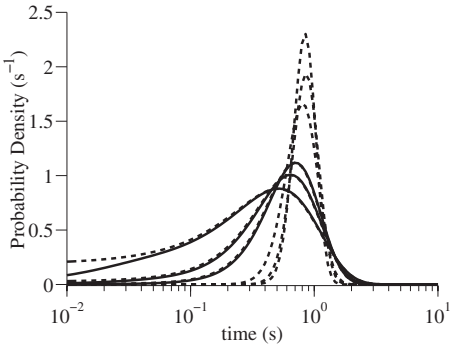


FIG. 10. Directly calculated probability density of the time until the number of refractory channels ($N_R$) increases to $N/2$, half the total number of channels in the release site model. Solid lines show the results obtained using the full model generator matrices for 8, 12, and 16 channels [sizes 165–969; see Eq. (5)]. Dashed lines show the results obtained using the fast/slow reduced generator matrix for 8, 12, 16, 40, 60, and 80 channels (sizes 9–81). In all calculations the initial probability distribution is the stationary distribution for $c_\infty=0.1\ \mu M$; at time zero this background $[Ca^{2+}]$ is increased to $c_\infty=0.35\ \mu M$. The coupling strengths were chosen so that $c_*N=0.52\ \mu M$ (e.g., in the eight channel case $c_*=0.065\ \mu M$).

open ($N_O$) and refractory ($N_R$) channels as a function of time in a stochastic simulation of a $Ca^{2+}$ release site composed of 60 independently gating Keizer–Levine RyRs ($c_*=0$). While the background $[Ca^{2+}]$ is initially $c_\infty=0.1\ \mu M$, this value is increased to 0.35 and 0.5 $\mu M$ at times indicated in the lower panel. Note that the increase in $N_O$ upon the second step in $[Ca^{2+}]$ corresponds to the phenomenon of "$Ca^{2+}$ adaptation" that is an important aspect of the paper that introduced the RyR model used here [cf. Fig. 2c in Ref. 21]. For comparison, the thick solid lines of Fig. 9 show results for a $Ca^{2+}$ release site composed of 60 *coupled* Keizer–Levine RyRs ($c_*=0.02\ \mu M$); interestingly, in this case adaptation is no longer observed.

More important to our present purposes are the broken lines of Fig. 9, which show exact results obtained from the probability distribution $\boldsymbol{\pi}(t)$ directly calculated using matrix exponentials of fast/slow reduced release generator matrices, that is,

$$\boldsymbol{\pi}(t)=\begin{cases}\boldsymbol{\pi}_0, & t<t_1,\\ \boldsymbol{\pi}_0 e^{(t-t_1)\hat{\boldsymbol{Q}}_1}, & t_1\le t<t_2,\\ \boldsymbol{\pi}_0 e^{(t_2-t_1)\hat{\boldsymbol{Q}}_1} e^{(t-t_2)\hat{\boldsymbol{Q}}_2}, & t_2\le t,\end{cases} \tag{20}$$

where $\boldsymbol{\pi}_0\hat{\boldsymbol{Q}}_0=\mathbf{0}$ subject to $\boldsymbol{\pi}_0\boldsymbol{e}=1$, and $\hat{\boldsymbol{Q}}_0$, $\hat{\boldsymbol{Q}}_1$, and $\hat{\boldsymbol{Q}}_2$ are generator matrices reduced from the full model evaluated with $c_\infty=0.1$, 0.35, and 0.5 $\mu M$, respectively. While it is possible to obtain similar results by performing many Monte Carlo simulations and averaging, direct numerical calculation is computationally more efficient because the matrix exponential calculations of Eq. (20) use the 61-state reduced generator matrix ($0\le N_R\le N$) as opposed to the 39 711-state full model [$\beta(60,4)$ in Eq. (5)].

Figure 10 gives another example of how automated fast/slow reduction can be used in conjunction with matrix analytic formulas to probe the stochastic dynamics of $Ca^{2+}$ release sites, the size of which would otherwise make direct numerical calculations unfeasible and Monte Carlo simulation inefficient and unreliable. Using $N=8$, 12, and 16 channels, the solid lines of Fig. 10 present direct calculations of the probability density of the time until the number of refractory channels ($N_R$) increases to $N/2$, half the total number of channels in the release site model. These were calculated by permuting the generator matrix of the full model into the following form:

$$Q=\begin{pmatrix}Q_{aa} & Q_{ab}\\ Q_{ba} & Q_{bb}\end{pmatrix}, \tag{21}$$

where each partition contains rates for transitions between (or within) aggregate classes of states where $N_R<N/2$ $(a)$ and $N_R\ge N/2$ $(b)$. The probability distribution is given by[36,37]

$$f(t)=-\phi_a e^{tQ_{aa}}Q_{aa}\boldsymbol{e}_a>0, \tag{22}$$

where $\boldsymbol{e}_a$ is a commensurate column vector of ones, $\phi_a$ is a row vector giving the initial probabilities of each state, and for simplicity we assume $\phi_a=\boldsymbol{\pi}_a/\boldsymbol{\pi}_a\boldsymbol{e}_a$, where $\boldsymbol{\pi}=(\boldsymbol{\pi}_a\ \boldsymbol{\pi}_b)$ is the stationary distribution solving $\boldsymbol{\pi}Q=\mathbf{0}$. The dashed lines of Fig. 10 repeat these calculations using the generator matrix for the fast/slow reduced model. Not only does the agreement validate the reduction method, but perhaps more importantly, by using the fast/slow reduced generator matrix we are able to calculate the distributions for release sites composed of 40, 60, and 80 channels (dashed lines). Because the matrix exponential in Eq. (22) must be calculated for many different values of $t$, full model calculations are extremely time consuming if not impossible due to storage limitations. On the other hand, calculating the matrix exponentials in the reduced model case takes less than a second. While performing the model reduction using the IAD-based reduction method (Algorithm 4) is overhead, this step need be performed only once.

## IX. DISCUSSION

We have implemented and validated several numerical procedures for reducing compositionally defined calcium release site models through fast/slow analysis. In all the approaches presented here, rate constants in the single channel model are categorized as either fast or slow, groups of states in the release site model that are connected by fast transitions are identified and lumped, and transition rates between reduced states are chosen consistent with exact or approximate conditional probability distributions among states within each group. For $Ca^{2+}$ release site models that are small enough to allow direct calculation of the stationary distribution of the full model, Algorithm 3 is preferred in spite of its substantial storage requirements because the exact conditional probability distributions result in a reduced model that is natural for the chosen partitioning of states. For release sites composed of many channels, the conditional probability distributions can be approximated without the construction of the full model by assuming a rapid mixing of states connected by fast transitions (Algorithms 1 and 2). Alternatively, an IAD method can be employed to obtain a reduced $Ca^{2+}$ release site model in a memory-efficient fashion.

We compared the convergence properties of reduction algorithms using three IAD methods: KMS, Vantilborgh, and Takahashi.[34,35] Our results suggest that KMS IAD-based reduction method is superior in the context of $Ca^{2+}$ release site modeling (Algorithm 4). Calculations performed using Vantilborgh IAD required more iterations to converge than KMS, while those using the Takahashi method often did not converge (not shown). Note that memory-efficient implementation of model reduction using Algorithm 4 begins with enumeration of the state space of a full $Ca^{2+}$ release site model. This preliminary step must also be performed without excessive storage requirements (see Appendix B and Algorithms 5 and 6).

We were able to validate Algorithms 1–4 by confirming that the transition probability matrix of the reduced model well approximates the corresponding contraction of the full model transition probability matrix, provided the separation of time scales between fast and slow processes is large enough (Figs. 6 and 8). As expected, both Algorithms 1 and 2 yield more error than the memory-inefficient reduction that uses the exact conditional probability distributions (Algorithm 3). Note that the KMS IAD-based Algorithm 4produces the same reduced model as Algorithm 3. The essential difference between Algorithms 3 and 4 is the numerical scheme used to calculate the exact conditional probability distributions. Because Algorithm 3 is not tractable for large $Ca^{2+}$ release site models, we recommend Algorithm 4 to investigators interested in $Ca^{2+}$ release site model reduction based on a separation of time scales.

It is important to note that while we have validated the four model reduction procedures presented here (Algorithms 1–4), the performance of a particular reduced model is a complicated matter that will depend on the single channel model used and, of course, the choice of parameters that influence the time scale separation of transitions identified as fast and slow.

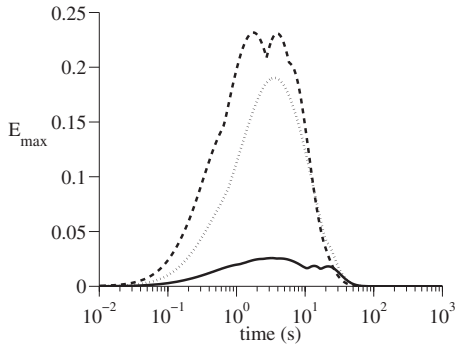


FIG. 11. Reduction error of gold standard reduction procedure (Algorithm 3) for release sites composed of 8 (solid line), 12 (dotted line), and 16 (dashed line) four-state Keizer–Levine RyRs. $c_\infty=0.1\ \mu M$, $c_*=0.065\ \mu M$, and other parameters as in Fig. 1.

While the error measure based on transition probability matrices [Eq. (15)] is sufficient for our present purposes, we have not yet performed a detailed study of puff/spark duration and interevent interval in full and reduced $Ca^{2+}$ release site models. The extent to which model reduction may perturb measures of particular relevance to the stochastic dynamics of $Ca^{2+}$ release is a question that deserves further consideration. Because puff/spark statistics are coarser measures of release site dynamics than the transition probability matrix itself, a reduced model could perform well with respect to the distribution of spark durations (for example), even when $\hat{E}_{\max}(t)$ is not promising. While it is of some concern that $\hat{E}_{\max}(t)$ often grows with the number of channels (Fig. 11), this does not adversely affect the reduced model probability densities of Fig. 10.

Although beyond the scope of this paper, Algorithm 4 can be implemented in a distributed parallel fashion. Such implementation would likely be required to perform fast/slow reduction when $Ca^{2+}$ release sites are composed of single channel models with many states. For example, a De Young–Keizer-like $IP_3R$ model[22] that includes four independent eight-state subunits—each with one binding site for $IP_3$ and two binding sites for $Ca^{2+}$—results in a single channel model with $\beta(4,8)=330$ distinguishable states [Eq. (5)]. Assuming fast $IP_3$-potentiation, fast $Ca^{2+}$-activation, and slow $Ca^{2+}$-inactivation, the topology of the fast and slow transitions results in two groups of four states for each subunit. This results in five groups with 35, 80, 100, 80, and 35 states for the single channel model, that is, $\beta(n_{\text{disinact}},4)\beta(n_{\text{inact}},4)$ for $n_{\text{inact}}=0,1,2,3,4$ and $n_{\text{inact}}+n_{\text{disinact}}=4$. Assuming a release site composed of $N$ De Young–Keizer-like $IP_3Rs$, Fig. 12 shows the state space size of the full model (solid line) and the size of the largest (dashed line) and average (dotted line) diagonal block [cf. Eq. (10)]. Note that the limiting slopes for the De Young–Keizer $IP_3R$ are much greater than those observed for the Keizer–Levine RyR. For the Keizer–Levine RyR, the number of states in the full model is $\beta(N,4)\sim N^3$ and the largest block size is $\beta(N,3)\sim N^2$ (all channels in the largest group that includes three states; see Fig. 2). For the De Young–Keizer-like $IP_3R$, the number of states in the full model is $\mathcal{O}(N^{330})$ and the largest block size is $\mathcal{O}(N^{326})$ (326=330 states−5 groups+1).

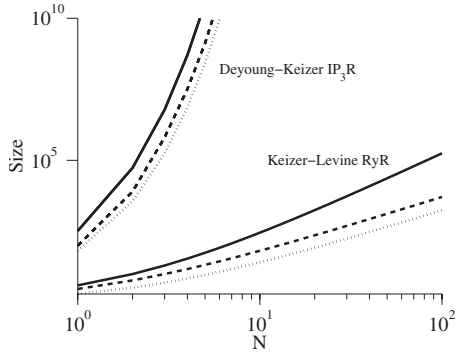


FIG. 12. State space size [Eq. (5)] of the full $Ca^{2+}$ release site model (solid line), size of the largest (dashed line) and average (dotted line) diagonal block of the partitioned generator matrix for $1 \le N \le 100$ four-state Keizer–Levine RyRs (see Fig. 4). The reduced release site model has $\hat{b}=N+1$ states (not shown) because slow transitions in the Keizer–Levine RyR separate two groups of states (Fig. 2).

Throughout this paper we assume that the fast and slow transitions of the single channel model are identified by the modeler, and this specification is used to partition the full model generator matrix (cf. Fig. 2). While this makes sense given the likely prior understanding of time scales of single channel kinetics, this approach neglects the effect of $[Ca^{2+}]$ changes on separation of time scales. That is, a $Ca^{2+}$-dependent transition such as $C_1 \to O_2$ or $O_2 \to O_3$ in the Keizer–Levine RyR may be slow or fast depending on $N_O(t)$. While the memory-efficient Algorithm 4 leads to the gold standard reduced model for any given partitioning, the approach to partitioning used here may not be optimal. In fact, when a 165-state release site is reduced to nine states as in Figs. 5–8, there are $\beta(9165) \approx 3 \times 10^{14}$ possible partitioning schemes. Given the separation of time scales in the Keizer–Levine RyR, the chosen partitioning scheme is presumably among the best, but it is unclear how to demonstrate this without enumerating all the possibilities and comparing reduction errors. An important topic for future work is automated determination of the optimal partitioning of a full model generator matrix to achieve a target number of reduced model states. In cases where the reduction error is defined in terms of a puff/spark statistic of interest (e.g., spark duration), the optimal partitioning schemes would presumably be sensitive to the aggregate classes of states being lumped (e.g., closed versus open) as well as separation of time scales.[20] In future work we hope to combine the automated fast/slow reduction procedure presented here with whole cell modeling techniques that include a probability density-based description of the local $[Ca^{2+}]$ experienced by clusters of intracellular and plasma membrane $Ca^{2+}$ channels.[38,39]

## ACKNOWLEDGMENTS

This material is based upon the work supported by the National Science Foundation under Grant No. 0443843. The authors acknowledge stimulating discussions with H. Drew LaMar, Ruth Lamprecht, and Ryan Carpenter. This project was initially conceived during collaborative work with George S. B. Williams, Marco A. Huertas, M. Saleet Jafri, and Eric A. Sobie (Refs. 38 and 39).

## APPENDIX A: IMPLEMENTATION OF FAST/SLOW REDUCTION PROCEDURES

Algorithms 1–6 were implemented in MATLAB (The MathWorks, Inc.). Equations of the form $\boldsymbol{xA}=\boldsymbol{0}$ subject to $\boldsymbol{xe}=1$ were solved by evaluating $\boldsymbol{x} \leftarrow (\boldsymbol{0}\ \ 1)/(\boldsymbol{A}\ \ \boldsymbol{e})$ where the slash corresponds to MATLAB's MRDIVIDE command. When solving an equation of the form $\boldsymbol{xP}=\lambda\boldsymbol{x}$ subject to $\boldsymbol{xe}=1$ we used MATLAB's EIGS command to find the eigenvector corresponding to the eigenvalue with largest real part and then normalized the result. In our implementation of Algorithm 4, the aggregation and disaggregation steps were solved using EIGS and MLDIVIDE, in spite of the fact that the aggregated system for nearly completely decomposable Markov chains is expected to be ill conditioned (Ref. 33, pages 321–322). It is possible that the inferior performance of the Takahashi method could be improved with a different implementation of these steps (Table I).

## APPENDIX B: GENERATION OF STATE SPACE AND BLOCKS OF PARTITIONED FULL MODEL

Instantaneous mean-field coupling of $N$ identical $M$-state channels yields a $Ca^{2+}$ release site model with $\beta(N,M)$ states where

$$\beta(N,M) = \binom{N+M-1}{N} = \frac{(N+M-1)!}{N!\,(M-1)!}.$$

Assuming transitions in the single channel model are labeled fast or slow in a manner that results in $L$ groups of states of size $m_1, m_2, \ldots, m_L$ with $\Sigma_{i=1}^{L} m_i = M$, the partitioned matrix corresponding to Eq. (10) will have $\beta(N,L)$ blocks, each of which can be labeled as $n_1 n_2 \cdots n_L$ indicating $n_i$ channels in group $i$ where $\Sigma_{i=1}^{L} n_i = N$. The diagonal block corresponding to macrostate $n_1 n_2 \cdots n_L$ is a square matrix of size

$$\prod_{i=1}^{L} \binom{n_i + m_i - 1}{n_i}.$$

An important aspect of the memory-efficient model reduction approach of Algorithm 4 is construction of the $\hat{b}^2$ input matrices $\{\boldsymbol{Q}_{ij}\}$. To ensure that the storage requirements of specifying the full model are not limiting, it is helpful to construct the $\boldsymbol{Q}_{ij}$ independently. This was accomplished using a recursive function $\mathbb{B}(nball, nbin)$ that returns a matrix enumerating (in antilexicographical order) the number of ways that *nball* indistinguishable items can be arranged in *nbin* distinguishable locations (Algorithm 5). For example, the full state space for two four-state channels is the $10 \times 4$ matrix

$$\mathbb{B}(2,4) = \begin{bmatrix} 2 & 0 & 0 & 0 \\ 1 & 1 & 0 & 0 \\ 1 & 0 & 1 & 0 \\ 1 & 0 & 0 & 1 \\ \vdots & \vdots & \vdots & \vdots \\ 0 & 0 & 0 & 2 \end{bmatrix}. \tag{B1}$$

**Algorithm 5:** $\mathbb{B}(nball,nbin)$ Recursive state space generation
**require:** *nball*, *nbin*
**if** $nbin=1$ **return** *nball*
**if** $nball=0$ **return** $1\times nbin$ matrix of zeros
$\boldsymbol{B}\leftarrow\emptyset$ (an empty matrix)
**for** $\ell=nball,nball-1,\cdots,0$
  $\boldsymbol{B}_R=\mathbb{B}(nball-\ell,nbin-1)$
  $\boldsymbol{B}_L\leftarrow$column vector of $\ell$'s with same number of rows as $\boldsymbol{B}_R$
  $\boldsymbol{B}\leftarrow[\boldsymbol{B};\boldsymbol{B}_L\boldsymbol{B}_R]$
**endfor**
**return** $\boldsymbol{B}$

When the state space of the full model ($\mathbb{B}(N,M)$) is large, the state space of the reduced model ($\mathbb{B}(N,L)$) is constructed instead, where $L$ is the number of groups of states separated by slow transitions ($L<M$). Denoting the rows of $\mathbb{B}(N,L)$ as $\{n_1n_2\cdots n_L\}$ where $n_1=0,1,\ldots,m_1$, $n_2=0,1,\ldots,m_2$, etc., the states in the full model that compose any particular lumped state $n_1n_2\cdots n_L$ can be enumerated as follows:

$$\begin{bmatrix} \mathbb{B}_1(n_1,m_1) & \mathbb{B}_1(n_2,m_2) & \cdots & \mathbb{B}_1(n_L,m_L) \\ \mathbb{B}_1(n_1,m_1) & \mathbb{B}_1(n_2,m_2) & \cdots & \mathbb{B}_2(n_L,m_L) \\ \vdots & \vdots & & \vdots \\ \mathbb{B}_1(n_1,m_1) & \mathbb{B}_1(n_2,m_2) & \cdots & \mathbb{B}_K(n_L,m_L) \\ \mathbb{B}_1(n_1,m_1) & \mathbb{B}_2(n_2,m_2) & \cdots & \mathbb{B}_1(n_L,m_L) \\ \vdots & \vdots & & \vdots \\ \mathbb{B}_K(n_1,m_1) & \mathbb{B}_K(n_2,m_2) & \cdots & \mathbb{B}_K(n_L,m_L) \end{bmatrix},$$

where $\mathbb{B}_k(n_\ell,m_\ell)$ indicates the $k$th row of $\mathbb{B}(n_\ell,m_\ell)$ and an upper case $K$ indicates the final row.

With the subset of the full model state space corresponding to a particular lumped state $n_1n_2\cdots n_L$ available, it is possible to construct the blocks $\boldsymbol{Q}_{ij}$ of the partitioned full model without knowledge on the entire state space. This is accomplished using Algorithm 6, which takes as input a matrix $\boldsymbol{B}$ corresponding to a set of states and returns as output the matrix $\mathbb{R}(\boldsymbol{B})=\boldsymbol{R}=(r_{k\ell})$, where the $r_{k\ell}$ are nonzero if and only if a transition is possible between states $\boldsymbol{B}_k$ and $\boldsymbol{B}_\ell$ and, when a transition is possible, the origin and destination states of the one channel that changes state are $r_{k\ell}$ and $r_{\ell k}$, respectively. For example, focusing on the subsequence of rows of Eq. (B1) corresponding to zero inactivated channels ($N_{C_2}=0$),

$$\boldsymbol{B}=\begin{bmatrix} 2 & 0 & 0 & 0 \\ 1 & 1 & 0 & 0 \\ 1 & 0 & 1 & 0 \\ 0 & 2 & 0 & 0 \\ 0 & 1 & 1 & 0 \\ 0 & 0 & 2 & 0 \end{bmatrix},$$

the function $\mathbb{R}(\boldsymbol{B})$ evaluates to

$$\mathbb{R}(\boldsymbol{B})=\begin{bmatrix} 0 & 1 & 1 & 0 & 0 & 0 \\ 2 & 0 & 2 & 1 & 1 & 0 \\ 3 & 3 & 0 & 0 & 1 & 1 \\ 0 & 2 & 0 & 0 & 2 & 0 \\ 0 & 3 & 2 & 3 & 0 & 2 \\ 0 & 0 & 3 & 0 & 3 & 0 \end{bmatrix}. \tag{B2}$$

The diagonal block of the full model corresponding to transitions within states of $\boldsymbol{B}$ is then given by

$$\boldsymbol{Q}_{\boldsymbol{BB}}=\begin{bmatrix} \cdot & q_{12} & q_{13} & \cdot & \cdot & \cdot \\ q_{21} & \cdot & q_{23} & q_{12} & q_{13} & \cdot \\ q_{31} & q_{32} & \cdot & \cdot & q_{12} & q_{13} \\ \cdot & q_{21} & \cdot & \cdot & q_{23} & \cdot \\ \cdot & q_{31} & q_{21} & q_{32} & \cdot & q_{23} \\ \cdot & \cdot & q_{31} & \cdot & q_{32} & \cdot \end{bmatrix},$$

where the dots indicate zero, the $q_{ij}$ are the $i\rightarrow j$ transition rates of the single channel model that either do not depend on $[Ca^{2+}]$ or are evaluated using $N_O$ consistent with the relevant row of $\boldsymbol{B}$, and the indices for these transition rates are chosen by reading off the elements of $\mathbb{R}(\boldsymbol{B})$ and $\mathbb{R}(\boldsymbol{B})^T$. Off-diagonal blocks of the full model corresponding to transitions between two groups of states ($\boldsymbol{B}_-$ and $\boldsymbol{B}_+$) are found in a similar manner, beginning with the evaluation of

$$\mathbb{R}\left(\begin{bmatrix}\boldsymbol{B}_- \\ \boldsymbol{B}_+\end{bmatrix}\right)=\begin{bmatrix}\boldsymbol{R}_{--} & \boldsymbol{R}_{-+} \\ \boldsymbol{R}_{+-} & \boldsymbol{R}_{++}\end{bmatrix}$$

using Algorithm 6. The matrices $\boldsymbol{R}_{-+}$ and $\boldsymbol{R}_{-+}$ provide indices of the single channel model transition rates that need to produce $\boldsymbol{Q}_{\boldsymbol{B}_-\boldsymbol{B}_+}$ and $\boldsymbol{Q}_{\boldsymbol{B}_+\boldsymbol{B}_-}$.

**Algorithm 6:** $\mathbb{R}(\boldsymbol{B})$ Determine transition rates for a given block of the full model

**require:** origin and destination states $\boldsymbol{B}$
$n\leftarrow$number of rows of $\boldsymbol{B}$
$\boldsymbol{R}\leftarrow n\times n$ matrix of zeros
**for** $i=1,\cdots,n$
  **for** $j=i+1,i+2,\cdots,n$ **do**
    $\boldsymbol{\Delta}\leftarrow j$th row of $\boldsymbol{B}-i$th row of $\boldsymbol{B}$
    **if** $\boldsymbol{\Delta}$ contains exactly one $-1$ and one 1 **then**
      $\boldsymbol{R}(i,j)\leftarrow$index of the $-1$ in $\Delta$
      $\boldsymbol{R}(j,i)\leftarrow$index of the 1 in $\Delta$
    **endif**
  **endfor**
**endfor**
**return** $\boldsymbol{R}$

[1]M. J. Berridge, J. Physiol. (London) **499**, 291 (1997).
[2]M. J. Berridge, Neuron **21**, 13 (1998).
[3]H. Cheng, M. R. Lederer, W. J. Lederer, and M. B. Cannell, Am. J. Physiol. **270**, C148 (1996).
[4]H. Cheng, W. J. Lederer, and B. Mark, Science **262**, 740 (1993).
[5]I. Parker, J. Choi, and Y. Yao, Cell Calcium **20**, 105 (1996).
[6]I. Parker and Y. Yao, J. Physiol. (London) **491**, 663 (1996).
[7]Y. Yao, J. Choi, and I. Parker, J. Physiol. (London) **482**, 533 (1995).
[8]V. Nguyen, R. Mathias, and G. D. Smith, Bull. Math. Biol. **67**, 393 (2005).

[9]S. Swillens, G. Dupont, L. Combettes, and P. Champeil, Proc. Natl. Acad. Sci. U.S.A. **96**, 13750 (1999).
[10]H. DeRemigio and G. D. Smith, Cell Calcium **38**, 73 (2005).
[11]H. DeRemigio and G. D. Smith, IMA J. Math. Appl. Med. Biol. **25**, 65 (2008).
[12]J. R. Groff and G. D. Smith, Biophys. J. **95**, 135 (2008).
[13]M. A. Huertas and G. D. Smith, J. Theor. Biol. **246**, 332 (2007).
[14]S. Swillens, P. Champeil, L. Combettes, and G. Dupont, Cell Calcium **23**, 291 (1998).
[15]J. W. Shuai and P. Jung, Biophys. J. **83**, 87 (2002).
[16]J. Shuai, H. J. Rose, and I. Parker, Biophys. J. **91**, 4033 (2006).
[17]J. Shuai, J. E. Pearson, J. K. Foskett, D.-O. D. Mak, and I. Parker, Biophys. J. **93**, 1151 (2007).
[18]J. W. Shuai and P. Jung, Proc. Natl. Acad. Sci. U.S.A. **100**, 506 (2003).
[19]J. R. Groff and G. D. Smith, J. Theor. Biol. **253**, 483 (2008).
[20]H. DeRemigio, P. Kemper, M. D. LaMar, and G. D. Smith, Phys. Biol. **5**, 036003 (2008).
[21]J. Keizer and L. Levine, Biophys. J. **71**, 3477 (1996).
[22]G. W. De Young and J. Keizer, Proc. Natl. Acad. Sci. U.S.A. **89**, 9895 (1992).
[23]Y. X. Li and J. Rinzel, J. Theor. Biol. **166**, 461 (1994).
[24]R. Hinch, Biophys. J. **86**, 1293 (2004).
[25]D. Colquhoun and A. G. Hawkes, in *Single-Channel Recording*, edited by B. Sakmann and E. Neher (Plenum, New York, 1995), pp. 589–633.
[26]G. D. Smith, in *Computational Cell Biology*, edited by C. P. Fall, E. S. Marland, J. M. Wagner, and J. J. Tyson (Springer-Verlag, Berlin, 2002), pp. 291–325.
[27]D. T. Gillespie, J. Phys. Chem. **81**, 2340 (1977).
[28]E. Niggli, Annu. Rev. Physiol. **61**, 311 (1999).
[29]X. P. Sun, N. Callamaras, J. S. Marchant, and I. Parker, J. Physiol. (London) **509**, 67 (1998).
[30]J. R. Groff, H. DeRemigio, and G. D. Smith, in *Stochastic Methods in Neuroscience*, edited by C. Laing and G. Lord (Oxford University Press, New York, 2009).
[31]T. L. Hill, *Free Energy Transduction in Biology and Biochemical Cycle Kinetics* (Springer-Verlag, Berlin, 1989).
[32]V. Nicola, "Lumping in Markov reward processes," IBM Thomas Watson Research Centre Report No. RC14719, 1998.
[33]W. J. Stewart, *Introduction to the Numerical Solution of Markov Chains* (Princeton University Press, Princeton, NJ, 1994).
[34]J. Koury, D. McAllister, and W. Stewart, SIAM J. Algebraic Discrete Methods **5**, 164 (1984).
[35]W. L. Cao and W. Stewart, J. Assoc. Comput. Mach. **32**, 702 (1985).
[36]F. Ball and Y. Geoffrey, Methodol. Comput. Appl. Probab. **2**, 93 (2000).
[37]F. G. Ball, R. K. Milne, and G. F. Yeo, IMA J. Math. Appl. Med. Biol. **17**, 263 (2000).
[38]G. S. B. Williams, M. A. Huertas, E. A. Sobie, M. S. Jafri, and G. D. Smith, Biophys. J. **92**, 2311 (2007).
[39]G. S. B. Williams, M. A. Huertas, E. A. Sobie, M. S. Jafri, and G. D. Smith, Biophys. J. **95**, 1689 (2008).